

# **Universal domain wall dynamics under electric field in Ta/Co<sub>40</sub>Fe<sub>40</sub>B<sub>20</sub>/MgO devices with perpendicular anisotropy**

Weiwei Lin<sup>1\*</sup>, Nicolas Vernier<sup>1</sup>, Guillaume Agnus<sup>1</sup>, Karin Garcia<sup>1</sup>, Berthold Ocker<sup>2</sup>,  
Weisheng Zhao<sup>1</sup>, Eric E. Fullerton<sup>3</sup> and Dafiné Ravelosona<sup>1\*</sup>

Electric field effects in ferromagnetic/oxide dielectric structures provide a new route to control domain wall (DW) dynamics with low power dissipation. However, electric field effect on DW velocity has been only observed so far in the creep regime where DW velocity is low due to a strong interaction with pinning sites. Here, we show gate voltage modulation of DW velocity within the creep, intermediate depinning, depinning and flow regimes with velocities up to 20 m s<sup>-1</sup> in Ta/Co<sub>40</sub>Fe<sub>40</sub>B<sub>20</sub>/MgO/TiO<sub>2</sub> structures with perpendicular magnetic anisotropy. We demonstrate a universal description of this effect over the full range of DW dynamics by taking into account an effective magnetic field being linear with the electric field. Our work opens new opportunities for the study and optimization of electric field effect at ferromagnetic metal/insulator interfaces.

---

<sup>1</sup>Institut d'Electronique Fondamentale, Université Paris-Sud - CNRS, UMR8622, Orsay 91405, France, <sup>2</sup>Singulus Technologies AG, Kahl am Main 63796, Germany, <sup>3</sup>Center for Magnetic Recording Research, University of California San Diego, La Jolla, California 92093, USA. \*email: [linwei613@gmail.com](mailto:linwei613@gmail.com) (W.L.), [dafine.ravelosona@u-psud.fr](mailto:dafine.ravelosona@u-psud.fr) (D.R.).

Electric field control of magnetic DW motion in transition metal ferromagnets<sup>1–7</sup> has attracted great interest due to the possibility to achieve DW control with low power dissipation for memory and logic circuits. One important example is racetrack memory<sup>8</sup>, where a gate voltage can be exploited to assist manipulation of DWs under spin-polarized currents<sup>1</sup>. This would allow the reduction of the generally large critical currents needed to depin and shift DWs in narrow wires. Another example concerns DW logic circuits<sup>9</sup>, for which local modulation of DW motion can lead to programmable DW energy landscapes. In both cases, the key is whether the electric field enables both efficient depinning for stored DWs and control of DW propagation.<sup>7</sup>

Materials with perpendicular magnetic anisotropy (PMA) are particularly attractive for DW devices as they exhibit narrow DWs<sup>10</sup> enabling high density storage. Recently, the electric field effect on DW dynamics has been demonstrated in Pt/Co/oxide films with PMA involving oxides with relatively high dielectric constant such as  $\text{AlO}_x$ <sup>3,6</sup>,  $\text{HfO}_2$ <sup>4</sup> or  $\text{GdO}_x$ <sup>5</sup>. However, significant modulation of DW velocity under gate voltage has been shown only in the creep regime where DWs propagate at relatively low speeds ( $< 0.1 \text{ m s}^{-1}$ ) through thermal activation over local energy barriers<sup>3–6</sup> originating from the random disorder.<sup>10,11</sup> The efficient gate-voltage control in the creep regime has been explained in terms of modulation of the activation energy barriers<sup>3–6</sup> through voltage-induced changes of the interfacial magnetic anisotropy.<sup>12–16</sup> With increasing DW velocity in the creep regime, the electric field effect was found to be strongly reduced due to the decrease of the activation energies with applied magnetic fields.<sup>5</sup> So far, there has been no report on the experimental observation of electric field effects beyond the creep regime, particularly in the depinning and flow regimes.<sup>17–19</sup>

Here, we report the first observation of voltage modulation of DW motion over four different dynamical regimes where velocities range from  $10^{-8} \text{ m s}^{-1}$  to  $20 \text{ m s}^{-1}$ . In addition, we demonstrate that this behavior can be understood over the full range of DW dynamics by a single effective magnetic field resulting from the electric field. Our

approach makes use of Ta/CoFeB/MgO films with PMA, for which the density of pinning sites and the damping are very low<sup>20-22</sup> with respect to other PMA materials such as Co/Pt<sup>19,23</sup> or Co/Ni<sup>18,24</sup>. In addition, PMA at the CoFeB/MgO interface can be manipulated efficiently through gate-voltage control.<sup>15,16</sup> These materials are considered as the most promising not only for spin transfer torque magnetic random access memory (STT-MRAM)<sup>25,26</sup> but also for DW based memories<sup>27</sup>, since a combination of spin Hall effect and Dzyaloshinskii-Moriya interaction could lead to efficient DW propagation under current.<sup>28-30</sup>

In this study, DW velocity under electric field was measured in both as-grown and annealed Ta(5nm)/Co<sub>40</sub>Fe<sub>40</sub>B<sub>20</sub>(1nm)/MgO(2nm)/TiO<sub>2</sub>(20nm)/ITO using magneto-optic Kerr microscopy under combined electric and magnetic fields. By applying a top gate voltage  $V_G$  between the bottom Ta/CoFeB and top ITO electrodes (shown schematically in Fig. 1), electrons can either accumulate or deplete at the CoFeB/MgO interface. For the experiments shown, positive (negative) voltage corresponds to electron accumulation (depletion) at the CoFeB/MgO interface. Figures 2a-2f shows typical differential Kerr images of magnetic DW motion in applied perpendicular magnetic field pulses in an annealed CoFeB structure for various  $V_G$ . The dark regions indicate the motion of the DW under the magnetic field pulse. The right and left boundaries in the dark part of the image shows the DW position before and after, respectively, applying the magnetic field pulse. The  $V_G$  was applied in the region of the 50- $\mu$ m-wide ITO strip as indicated by the dashed rectangle. As shown in Figs. 2a–2c, at  $\mu_0 H = 2.6$  mT for  $\Delta t = 1$  s, the DW displacement below the ITO strip at  $V_G = -1$  V is smaller than that at  $V_G = 0$  V, while the DW displacement at  $V_G = 1$  V is larger. Similar behavior can be observed at  $\mu_0 H = 9$  mT for  $\Delta t = 27$  s (Figs. 2d–2f). One may notice from Figs. 2a and 2d that the DW displacement below the ITO strip for  $V_G < 0$  is smaller than that out of the ITO strip without the gate voltage, while in Figs. 2c and 2f, the DW displacement below the ITO strip ( $V_G > 0$ ) is larger than that out of the ITO strip. These results demonstrates that the DW velocities decrease as applying negative  $V_G$  and increase as applying positive  $V_G$ . For a higher field  $\mu_0 H = 28.7$  mT and for  $\Delta t = 9$  s (Fig. 2g–2i), the DW

displacement at  $V_G = 1.5$  V is slightly larger than that at  $V_G = -1.9$  V.

Figures 2j-2l shows the dependence of DW velocity on the gate voltage in the annealed sample for the same values of  $\mu_0 H$  shown in Figs. 2a-2i. In all field ranges the DW velocity increases linearly with  $V_G$ . In the low-field regime, the effect of gate voltage on DW velocity is found to be relatively large (factor of 10 from  $-2$  V to  $+1$  V at  $2.6$  mT) but it strongly decreases (factor of 1.1 from  $-2$  V to  $+1$  V at  $28.7$  mT) with increasing magnetic field.

To determine the role of voltage on the various dynamic regimes, Fig. 3 shows the dependence of DW velocity  $v$  on the applied magnetic field  $H$  for typical gate voltages  $V_G = -1.5$  V,  $0$  V and  $1.5$  V. For the annealed sample three DW dynamical regimes are observed in Fig. 3 including the creep, intermediate depinning and depinning regimes<sup>11,17,19,21</sup>. In all regimes the DW velocity increases (decreases) under positive (negative) voltage in this annealed sample. In the creep regime where  $\mu_0 H < 8$  mT (Fig. 3b), the DW velocity can be expressed as

$$v^{\text{creep}} \sim \exp \left[ -\frac{U_C}{k_B T} \left( \frac{H_{\text{dep}}}{H} \right)^{\frac{1}{4}} \right] \quad (1)$$

where  $U_C$  is a characteristic energy related to the disorder-induced pinning potential,  $k_B$  the Boltzmann constant,  $T$  the temperature, and  $H_{\text{dep}}$  the depinning field at which the Zeeman energy is equal to the DW pinning energy.<sup>11</sup> The exponent  $1/4$  fits the data well and is theoretically predicted for interactions of one-dimensional DWs with two-dimensional weak random disorder in thin magnetic films with PMA.<sup>11</sup> In agreement with Ref. 19, close below  $H_{\text{dep}}$  a critical depinning regime is observed for  $\mu_0 H > 12$  mT, where the velocity fits as

$$v^{\text{dep}} \sim (H - H_{\text{dep}})^{\frac{1}{4}} \quad (2)$$

This regime allows us to determine accurately the value of  $H_{\text{dep}}$  for the gate voltages  $V_G = -1.5$  V,  $0$  V and  $1.5$  V. We find respectively  $\mu_0 H_{\text{dep}}(-1.5 \text{ V}) = 12.9$  mT,  $\mu_0 H_{\text{dep}}(0 \text{ V}) = 11.7$  mT and  $\mu_0 H_{\text{dep}}(1.5 \text{ V}) = 11.2$  mT. These results are consistent with Fig. 2 where a negative (positive) voltage impedes (favors) DW motion. Note that by using the value of  $\mu_0 H_{\text{dep}}$  determined from Eq. (2) into Eq. (1), the characteristic energy  $U_C$

is found to be not dependent on the voltage. Between these two regimes for  $8 \text{ mT} < \mu_0 H < 12 \text{ mT}$ , an intermediate depinning regime occurs. As evidenced in Ref. 19, an thermally activated flux flow (TAFF) regime may exist where

$$v^{\text{TAFF}} \sim \exp \left[ \frac{U_c}{k_B T} \left( \frac{H}{H_{\text{dep}}} - 1 \right) \right] \quad (3)$$

However, although this equation seems to fit the data well, precaution has to be taken due to the limited range of magnetic field values in this regime.

In the following, we demonstrate that the gate voltage effect on DW motion can be considered as an effective magnetic field over the full range of DW dynamics. Since DW velocities depend on both applied magnetic field and gate voltage, we can define an effective magnetic field  $H_{\text{eff}}$  where  $v(H, V_G) = v(H_{\text{eff}}, V_G = 0)$ . By doing a precise analysis of each  $V(H, V_G)$  value (see S2), we find that that  $H_{\text{eff}}$  can be written as

$$H_{\text{eff}}(V_G, H) = (1 + LV_G)H \quad (4)$$

where the coefficient  $L$  is  $0.050 \pm 0.005 \text{ V}^{-1}$  for this sample. To illustrate this behavior, Fig. 4a shows  $v$  as a function of  $(1 + LV_G)H$  under typical  $V_G$  of  $-1.5 \text{ V}$ ,  $0 \text{ V}$  and  $1.5 \text{ V}$  respectively. The behavior in the DW creep regime is also shown in Fig. 4b where  $v$  (in logarithmic scale) is plotted against  $[(1 + LV_G)H]^{-1/4}$ . All the curves can be superimposed by considering the effective magnetic field instead of the applied magnetic field, indicating that a universal description given by Eq. 4 is applicable quantitatively over the full range of DW dynamics.

These results suggest that the electric field effect on DW velocity follows the magnetic field dependence of the DW velocity. Particularly, one may expect a reversal of the voltage effect in case of the DW velocity decreases with increasing the applied magnetic field. Next, we evidence the observation of such reversal of the voltage effect on DW velocity. Figure 5 shows DW velocity at high fields in an as-grown  $\text{Ta}(5\text{nm})/\text{Co}_{40}\text{Fe}_{40}\text{B}_{20}(1\text{nm})/\text{MgO}(2\text{nm})/\text{TiO}_2(20\text{nm})/\text{ITO}$  structure, for which the PMA is lower due to the amorphous character of the CoFeB layer<sup>19</sup>. In this case, the beginning of the flow regime occurs at lower fields than the annealed sample,

which allows us to observe the flow regime. As shown in Fig. 5a, the velocity  $v$  increases up to  $\mu_0 H < 27$  mT but then decreases for  $\mu_0 H > 27$  mT. This additional regime beyond the depinning regime corresponds to a negative DW mobility above the Walker breakdown that is hidden by the depinning regime<sup>17,18,21,31</sup>. For  $\mu_0 H < 27$  mT the DW velocity increases with positive  $V_G$ , as shown in Fig. 5b. Interestingly Fig. 5c shows that for  $\mu_0 H = 30.5$  mT in the negative mobility regime, instead the DW velocity decreases with the increase of  $V_G$ , indicating the reversal of the electric field effect. The results can be also fitted by Eq. 4 with the coefficient  $L$  is  $0.04 \pm 0.01$  V<sup>-1</sup> for this amorphous sample.

Recent experiments on electric field effect have focused on mechanism based on charge accumulation or band shifting at the metal-oxide interface that drives change of the interface anisotropy. In our structure, the dielectric layer consists of a 2 nm thick MgO (dielectric constant  $\epsilon_{\text{MgO}} \sim 9.7$ ) and 20 nm thick TiO<sub>2</sub> (dielectric constant  $\epsilon_{\text{TiO}_2} \sim 100$ ) films. A positive (negative) gate voltage of  $V_G = +1$  V ( $-1$  V) corresponds to an electric field of  $\sim 2.5 \times 10^8$  V m<sup>-1</sup> and an accumulation (depletion) of  $\sim 0.01$  electron per Co(Fe) atom at the CoFeB/MgO interface. Interestingly, it has been shown recently that electron accumulation can give rise to a reduction of PMA in Ta/CoFeB/MgO structures.<sup>15,16,32,33</sup> The results here show that electron accumulation under positive voltage at the CoFeB/MgO interface either increase (Fig. 4) or decrease (Fig. 5) the DW velocity, depending on the regime of DW motion. In the creep, intermediate depinning and depinning regime, the increase of DW velocity under positive voltage is consistent with a reduction of the energy barrier when the PMA decreases. In the Walker regime, the negative DW mobility is related to the DW width, which also depends on the PMA and may explain a variation of DW velocity under voltage. However, this picture of electric field induced magnetic anisotropy change cannot explain why DW dynamics can be described by a single effective magnetic field. Indeed, the DW velocity under voltage can be written as  $v(H, V_G) = v(H_{\text{eff}}, V_G = 0)$  with  $H_{\text{eff}}$  given by Eq. 4 over the full range of dynamics. Since in the four regimes, the dependence of DW velocity on magnetic anisotropy is distinct, the origin of the presence of an effective field  $H_{\text{eff}}$  is very unclear. We believe, that

additional mechanisms related to Dzyaloshinskii-Moriya interaction<sup>28,34,35</sup> that can be induced and/or tuned by electric field may play a role.

In conclusion, the possibility to control DW velocity up to the flow regime opens new perspective for low power spintronics applications such as solid state memories and logic devices.

## Methods

**Fabrication of Ta/CoFeB/MgO/TiO<sub>2</sub>/ITO structure.** The Ta(5 nm)/Co<sub>40</sub>Fe<sub>40</sub>B<sub>20</sub>(1 nm)/MgO(2 nm)/Ta(5 nm) films were deposited on Si/SiO<sub>2</sub> wafers by magnetron sputtering. Selected films were annealed at 300 °C for two hours. After etching the top 5 nm thick Ta layer, a 20 nm thick TiO<sub>2</sub> dielectric layer was sputtered on the Ta/CoFeB/MgO film (see S1). Finally, 100 nm thick sputtered ITO (In<sub>2</sub>O<sub>3</sub>:Sn) stripes with width ranging from 10 μm to 50 μm were patterned on top of the TiO<sub>2</sub> layer as the top electrode by optical lithography and lift-off process. ITO was used as the top electrode because it is not only a good electrical conductor (about 7 Ω<sup>-1</sup> m<sup>-1</sup> conductivity), but also is transparent for visible light, so that it is possible to use Kerr microscopy for visualizing magnetic domains. By applying a top gate voltage  $V_G$  between the bottom Ta/CoFeB and the top ITO, electrons can accumulate or deplete at the CoFeB/MgO interface. Here, positive (negative) gate voltage corresponds to electron accumulation (depletion) in the CoFeB layer. The leakage current was measured to be less than a few nAs for gate voltages  $V_G < 1.5$  V and less than 100 nA at the maximum gate voltage  $V_G$  of -2 V and thus, Joule heating influence on DW motion can be negligible.

**Magnetic domain wall velocity measurement by polar Kerr microscopy.** The polar Kerr microscopy was performed using a diode with the blue light (455 nm in wavelength) and a ×50 objective lens. The analyzer was set to about 87 degree (analyzer and polarizer almost crossed) and the exposure time was 2 s. To measure DW velocity under an applied perpendicular magnetic field  $H$ , we used the following procedures: first, the sample was saturated with a magnetic field of -20 mT fixed for more than 10 s. Second, several positive magnetic field pulses of +3 mT with duration of around 10 s were applied, until the nucleation of a single DW below the ITO strip was observed. A reference Kerr image was taken at zero applied magnetic field after the first set of magnetic field pulses. Third, another magnetic field pulse was applied resulting in a DW displacement. The amplitude of the second set of magnetic field pulses ranged from 0.6 mT to 35 mT and their durations  $\Delta t$  from 100 s



(long pulse) to 9  $\mu\text{s}$  (short pulse). The magnetic field pulse was generated from a coil with 1 cm diameter, which was fixed very close to the sample, and the rise time of magnetic field was about 4  $\mu\text{s}$ . After the second set of magnetic field pulses were applied, a second Kerr image was taken as soon as the magnetic field was back to zero. The DW displacement during  $\Delta t$  was obtained by the difference between the two Kerr images, which gave the DW velocity  $v$ . The velocity measured under the short magnetic field pulses was determined by the slope of the DW displacement vs. magnetic field pulse duration.

## References

1. Yamanouchi, M., Chiba, D., Matsukura, F., Ohno, H. Current-assisted domain wall motion in ferromagnetic semiconductors. *Jap. J. Appl. Phys.* **45**, 3854–3859 (2006).
2. Logginov, A. S. *et al.* Room temperature magnetoelectric control of micromagnetic structure in iron garnet films, *Appl. Phys. Lett.* **93**, 182510 (2008).
3. Schellekens, A. J., van den Brink, A., Franken, J. H., Swagten, H. J. M. & Koopmans, B. Electric-field control of domain wall motion in perpendicularly magnetized materials. *Nature Commun.* **3**, 847 (2012).
4. Chiba, D. *et al.* Electric-field control of magnetic domain-wall velocity in ultrathin cobalt with perpendicular magnetization. *Nature Commun.* **3**, 888 (2012).
5. Bauer, U., Emori, S. & Beach, G. S. D. Voltage-gated modulation of domain wall creep dynamics in an ultrathin metallic ferromagnet. *Appl. Phys. Lett.* **101**, 172403 (2012).
6. Bernand-Mantel, A. *et al.* Electric-field control of domain wall nucleation and pinning in a metallic ferromagnet. *Appl. Phys. Lett.* **102**, 122406 (2013).
7. Bauer, U., Emori, S. & Beach, G. S. D. Voltage-controlled domain wall traps in ferromagnetic nanowires. *Nature Nanotechnol.* **8**, 411–416 (2013).
8. Parkin, S. S. P., Hayashi, M. & Thomas, L. Magnetic domain-wall racetrack memory. *Science* **320**, 190–194 (2008).

9. Allwood, D. A. *et al.* Submicrometer ferromagnetic NOT gate and shift register. *Science* **296**, 2003–2006 (2002).
10. Ferré, J. in *Spin Dynamics in Confined Magnetic Structures I*, edited by B. Hillebrands and K. Ounadjela (Springer-Verlag Berlin Heidelberg, 2002), Vol. 83, p. 127.
11. Lemerle, S. *et al.* Domain wall creep in an Ising ultrathin magnetic film. *Phys. Rev. Lett.* **80**, 849–852 (1998).
12. Weisheit, M. *et al.* Electric field-induced modification of magnetism in thin-film ferromagnets. *Science* **315**, 349–351 (2007).
13. Maruyama, T. *et al.* Large voltage-induced magnetic anisotropy change in a few atomic layers of iron. *Nature Nanotechnol.* **4**, 158–161 (2009).
14. Niranjana, M. K., Duan, C.-G., Jaswal, S. S. & Tsymbal, E. Y. Electric field effect on magnetization at the Fe/MgO(001) interface. *Appl. Phys. Lett.* **96**, 222504 (2010).
15. Endo, M. *et al.* Electric-field effects on thickness dependent magnetic anisotropy of sputtered MgO/Co<sub>40</sub>Fe<sub>40</sub>B<sub>20</sub>/Ta structures. *Appl. Phys. Lett.* **96**, 212503 (2010).
16. Kita, K., Abraham, D. W., Gajek, M. J. & Worledge, D. C. Electric-field-control of magnetic anisotropy of Co<sub>0.6</sub>Fe<sub>0.2</sub>B<sub>0.2</sub>/oxide stacks using reduced voltage. *J. Appl. Phys.* **112**, 033919 (2012).
17. Metaxas, P. J. *et al.* Creep and flow regimes of magnetic domain-wall motion in ultrathin Pt/Co/Pt films with perpendicular anisotropy. *Phys. Rev. Lett.* **99**, 217208 (2007).
18. Yamada, K. *et al.* Influence of instabilities on high-field magnetic domain wall velocity in (Co/Ni) nanostrips. *Appl. Phys. Express* **4**, 113001 (2011).
19. Gorchon, J. *et al.* Pinning-dependent field-driven domain wall dynamics and thermal scaling in an ultrathin Pt/Co/Pt magnetic film. *Phys. Rev. Lett.* **113**, 027205 (2014).
20. Devolder, T. *et al.* Damping of Co<sub>x</sub>Fe<sub>80-x</sub>B<sub>20</sub> ultrathin films with perpendicular magnetic anisotropy. *Appl. Phys. Lett.* **102**, 022407 (2013).

21. Burrowes, C. *et al.*, Low depinning fields in Ta-CoFeB-MgO ultrathin films with perpendicular magnetic anisotropy. *Appl. Phys. Lett.* **103**, 182401 (2013).
22. Tetienne, J-P. *et al.*, Nanoscale imaging and control of domain wall hopping with a nitrogen vacancy center microscope, *Science* **344**, 1366 (2014).
23. Mizukami, S. *et al.*, Gilbert damping in perpendicularly magnetized Pt/Co/Pt films investigated by all-optical pump-probe technique. *Appl. Phys. Lett.* **96**, 152502 (2010).
24. Mizukami, S. *et al.*, Gilbert damping in Ni/Co multilayer films exhibiting large perpendicular anisotropy. *Appl. Phys. Express* **4**, 013005 (2011).
25. Ikeda, S. *et al.* A perpendicular-anisotropy CoFeB-MgO magnetic tunnel junction. *Nature Mater.* **9**, 721–724 (2010).
26. Worledge, D. C. *et al.* Spin torque switching of perpendicular Ta/CoFeB/MgO-based magnetic tunnel junctions. *Appl. Phys. Lett.* **98**, 022501 (2011).
27. Fukami, S. *et al.* Current-induced domain wall motion in perpendicularly magnetized CoFeB nanowire. *Appl. Phys. Lett.* **98**, 082504 (2011).
28. Thiaville, A., Rohart, S., Jué, E., Cros, V. & Fert, A. Dynamics of Dzyaloshinskii domain walls in ultrathin magnetic films. *Europhys. Lett.* **100**, 57002 (2012).
29. Ryu, K.-S., Thomas, L., Yang, S.-H. & Parkin, S. Chiral spin torque at magnetic domain walls. *Nature Nanotechnol.* **8**, 527–533 (2013).
30. Emori, S., Bauer, U., Ahn, S.-M., Martinez, E. & Beach, G. S. D. Current-driven dynamics of chiral ferromagnetic domain walls. *Nature Mater.* **12**, 611–616 (2013).
31. Schryer, N. L. & Walker, L. R. The motion of 180° domain walls in uniform dc magnetic fields. *J. Appl. Phys.* **45**, 5406 (1974).
32. Bonell, F. *et al.*, Reversible change in the oxidation state and magnetic circular dichroism of Fe driven by an electric field at the FeCo/MgO interface. *Appl. Phys. Lett.* **102**, 152401 (2013).
33. Wang, W. G., Li, M., Hageman, S. & Chien, C. L. Electric-field-assisted switching in magnetic tunnel junctions. *Nature Mater.* **11**, 64–68 (2012).
34. Dzyaloshinskii, I. Magnetoelectricity in ferromagnets. *Europhys. Lett.* **83**, 67001

(2008).

35. Upadhyaya, P. *et al.* Electric field induced domain-wall dynamics: Depinning and chirality switching. *Phys. Rev. B* **88**, 224422 (2013).

### **Acknowledgements**

This work was partly funded by the European Community's Seventh Framework Programme FP7 under grant agreement 257707 (MAGWIRE); the French Agence Nationale de la Recherche (ANR) through the projects ELECMADÉ, FRIENDS and DIPMEN; and by RTRA, C'Nano IdF and LABEX NanoSaclay. We thank T. Devolder and S. Eimer for experimental assistance, and J. V. Kim, J. P. Adam, L. Ranno, A. Marty, A. Bernand-Mantel, D. Givord, L. Herrera-Diez, J. P. Jamet and V. Jeudy for fruitful discussions.

### **Author contributions**

W.L. and D.R. designed the experiment. B.O. optimized the deposition of Ta/CoFeB/MgO/Ta film. W.L. fabricated the Ta/CoFeB/MgO/TiO<sub>2</sub>/ITO structures with the help of G.A. and K.G. W.L. and N.V. performed polar Kerr microscopy measurement and analyzed the data. W.L. gave the phenomenological physics description and wrote the manuscript. N.V., E.E.F. and D.R. contributed to the manuscript revision. W.Z. discussed the work. D.R managed the study.

### **Competing financial interests**

The authors declare no competing financial interests.

## Figure captions

### **Figure 1 Schematic of the experiment in Ta/Co<sub>40</sub>Fe<sub>40</sub>B<sub>20</sub>/MgO/TiO<sub>2</sub> structures.**

The gate voltage  $V_G$  is applied between the ITO strip and the CoFeB film. The magnetic field  $H$  is applied perpendicular to the film plane. Polar Kerr microscopy is used to image magnetic domains under magnetic and electric fields.

### **Figure 2 Magnetic domain wall displacement under various gate voltages and applied magnetic fields in an annealed Ta/CoFeB/MgO structure.**

The DW displacement is obtained from the difference between the polar Kerr images after and before magnetic field pulses. The right (left) boundary in the dark part in the image shows the DW position before (after) applying the magnetic field pulse, and the arrow indicates the direction of DW motion. Top gate voltage  $V_G$  is applied in the region indicated by the dashed rectangle. **a-c**, DW displacement at applied magnetic fields  $\mu_0 H$  of 2.6 mT with 1 s duration under voltage  $V_G$  of -1 V, 0 V and 0.8 V, respectively. **d-f**, DW displacement at  $\mu_0 H = 9$  mT with 27  $\mu$ s duration under voltage  $V_G$  of -1.8 V, 0 V and 1.5 V, respectively. **g-i**, DW displacement at  $\mu_0 H = 28.7$  mT with 9  $\mu$ s duration under voltage  $V_G$  of -1.9 V, 0 V and 1.5 V, respectively. **j-k**,  $V_G$  dependences of domain wall velocity  $v$  under magnetic fields  $\mu_0 H$  of 2.6 mT, 9 mT and 28.7 mT, respectively.

### **Figure 3 Magnetic DW velocity as a function of the applied magnetic field for different gate voltages in an annealed Ta/CoFeB/MgO structure.**

**a**, velocity as a function of  $H$  under voltages  $V_G$  of -1.5 V (open squares), 0 V (solid squares) and 1.5 V (open circles). **b**, velocity (in logarithmic scale) as a function of  $H^{1/4}$  under voltages  $V_G$  of -1.5 V (open squares), 0 V (solid squares) and 1.5 V (open circles). The points correspond to the experimental data, and the lines to the fitting (see text).

### **Figure 4 Dependence of the effective magnetic field on the gate voltage for different applied magnetic fields in an annealed Ta/CoFeB/MgO structure.**

**a**, Velocity  $v$  as a function of  $(1+LV_G)H$  under voltages  $V_G$  of -1.5 V (open squares), 0 V

(solid squares) and 1.5 V (open circles), where  $L = 0.05 \text{ V}^{-1}$ . **b**, Velocity  $v$  (in logarithmic scale) as a function of  $[(1+LV_G)H]^{-1/4}$  under voltages  $V_G$  of -1.5 V (open squares), 0 V (solid squares) and 1.5 V (open circles), where  $L = 0.05 \text{ V}^{-1}$ .

**Figure 5 Gate voltage effect on magnetic DW velocity in an as-deposited Ta/CoFeB/MgO structure. a**, Velocity  $v$  as a function of  $H$  without gate voltage. **b,c**,  $V_G$  dependences of velocity  $v$  under magnetic field  $\mu_0 H$  of 6.1 mT and 30.5 mT, respectively.

Figure 1

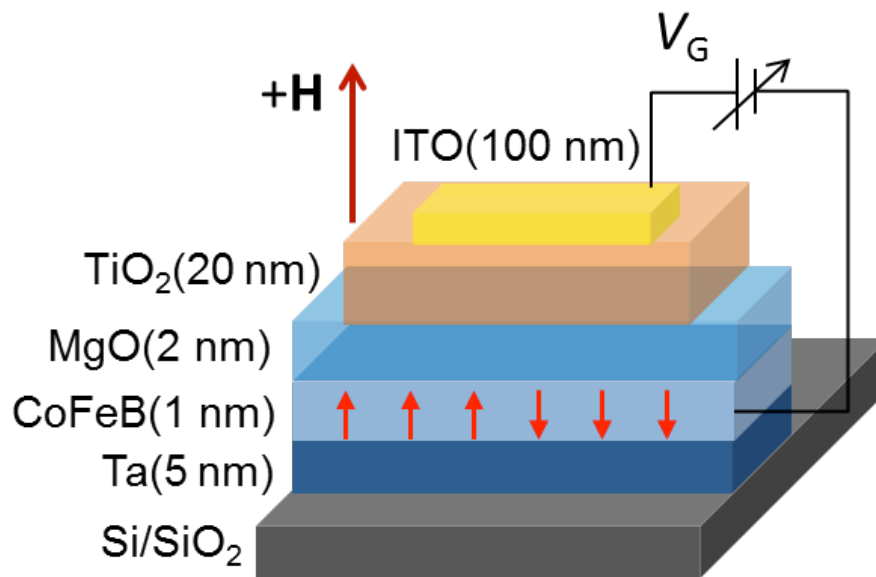


**Figure 2**

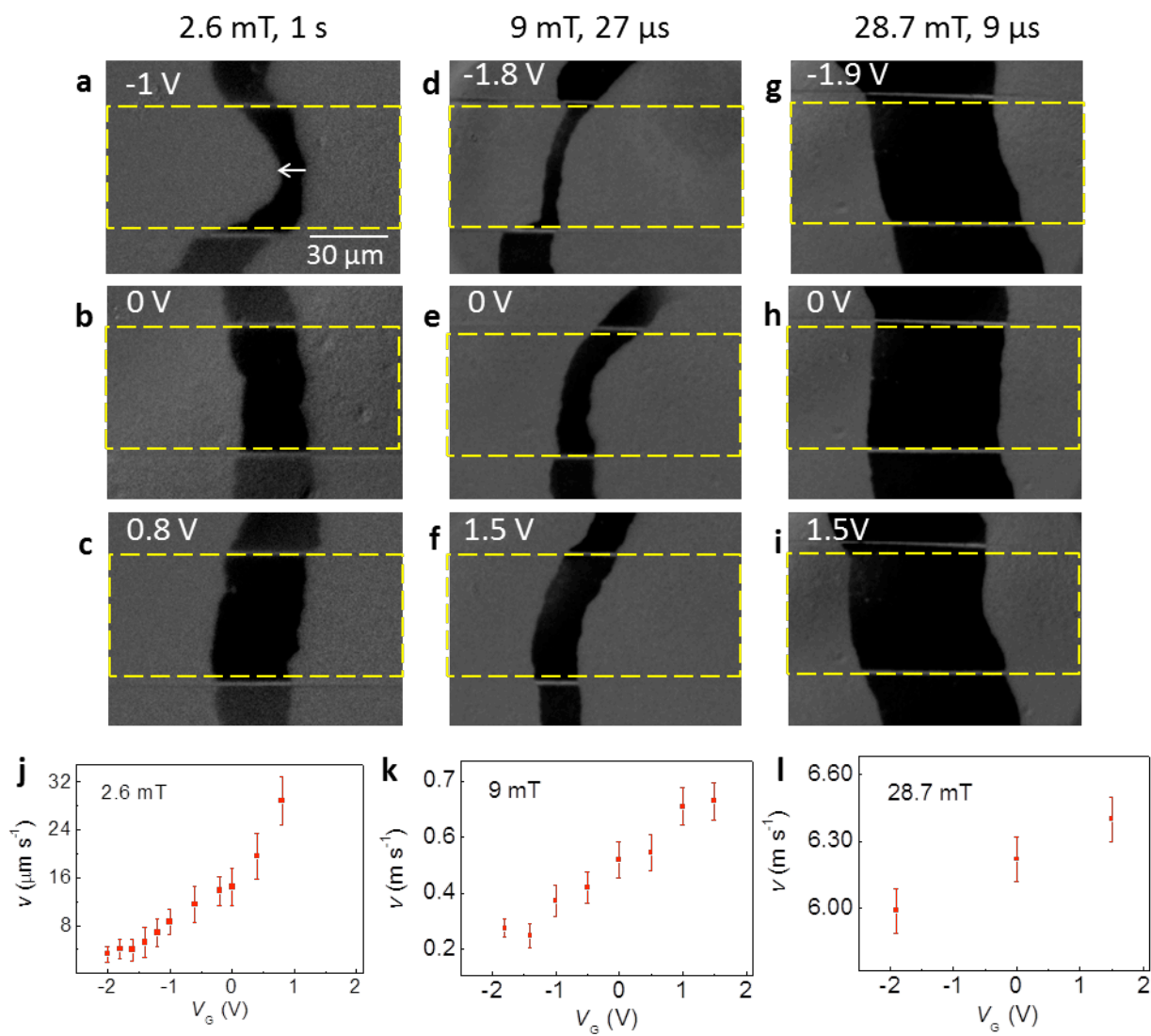




**Figure 3**

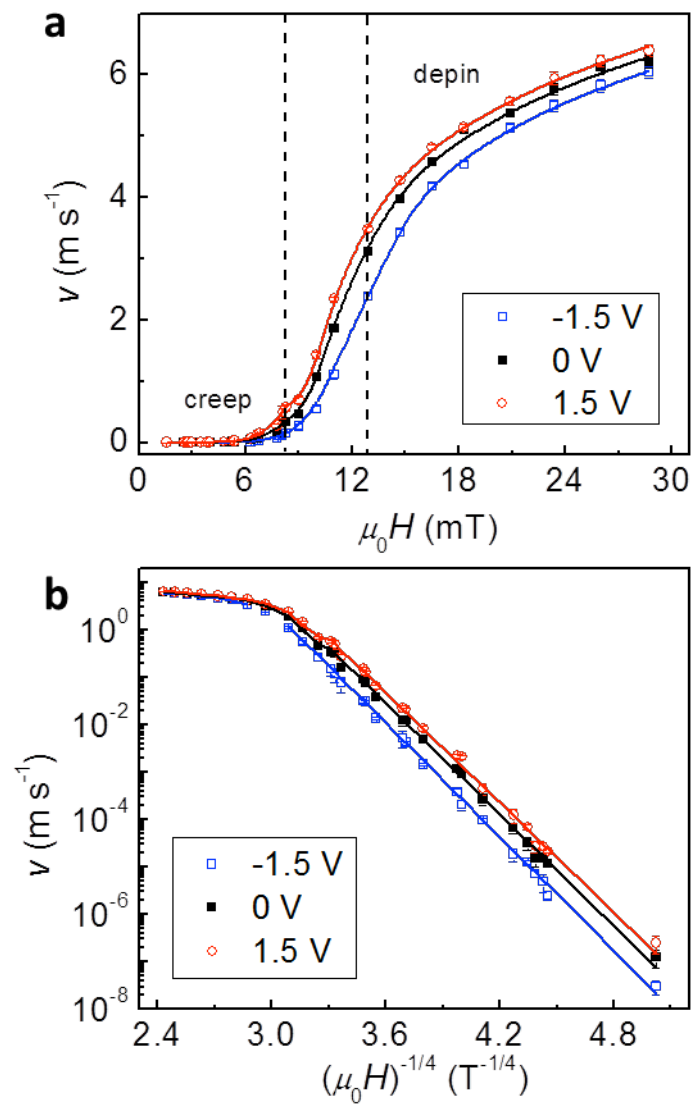


**Figure 4**

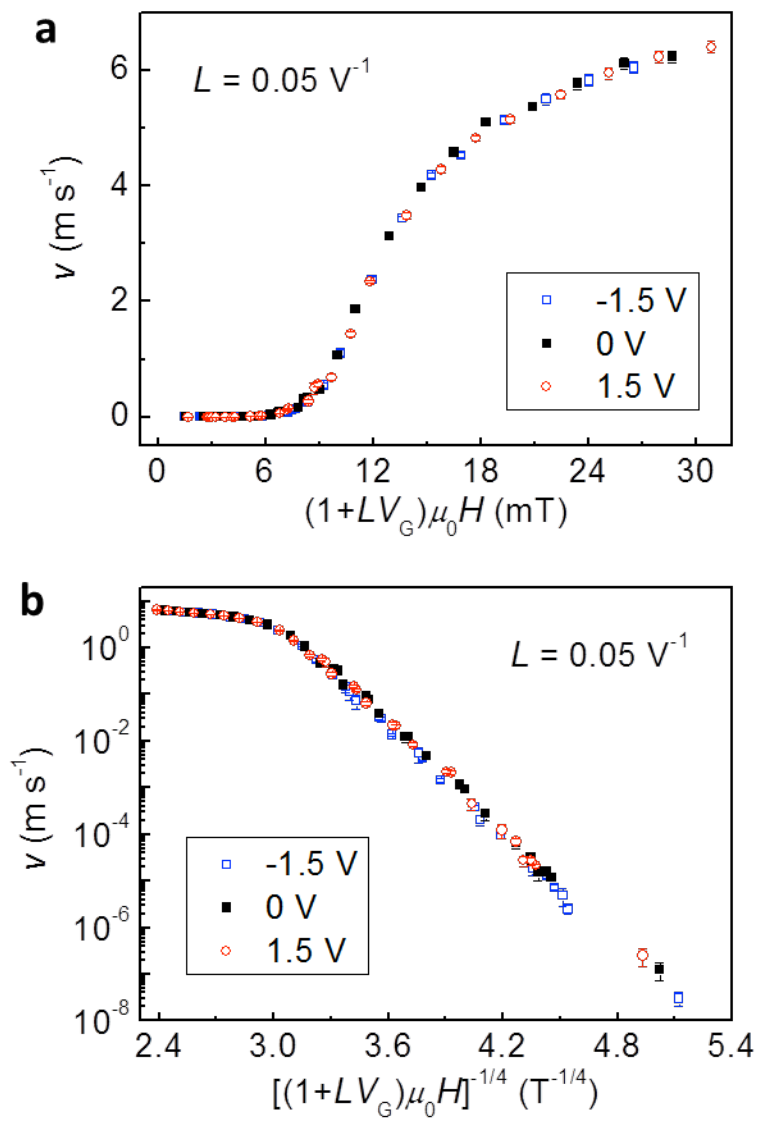


**Figure 5**

